



**HAL**  
open science

## 6-MeV Electron Exposure Effects on OFDR-Based Distributed Fiber-Based Sensors

Camille Sabatier, Serena Rizzolo, Adriana Morana, Timothé Allanche, Thierry Robin, Benoit Cadier, Philippe Paillet, Marc Gaillardin, Olivier Duhamel, Claude Marcandella, et al.

► **To cite this version:**

Camille Sabatier, Serena Rizzolo, Adriana Morana, Timothé Allanche, Thierry Robin, et al.. 6-MeV Electron Exposure Effects on OFDR-Based Distributed Fiber-Based Sensors. IEEE Transactions on Nuclear Science, 2018, 65 (8), pp.1598-1603. 10.1109/TNS.2018.2804663 . ujm-01926003

**HAL Id: ujm-01926003**

**<https://ujm.hal.science/ujm-01926003>**

Submitted on 15 Feb 2019

**HAL** is a multi-disciplinary open access archive for the deposit and dissemination of scientific research documents, whether they are published or not. The documents may come from teaching and research institutions in France or abroad, or from public or private research centers.

L'archive ouverte pluridisciplinaire **HAL**, est destinée au dépôt et à la diffusion de documents scientifiques de niveau recherche, publiés ou non, émanant des établissements d'enseignement et de recherche français ou étrangers, des laboratoires publics ou privés.



## Open Archive Toulouse Archive Ouverte (OATAO)

OATAO is an open access repository that collects the work of some Toulouse researchers and makes it freely available over the web where possible.

This is an author's version published in: <https://oatao.univ-toulouse.fr/22008>

**Official URL:** <https://doi.org/10.1109/TNS.2018.2804663>

### To cite this version :

Sabatier, Camille and Rizzolo, Serena and Morana, Adriana,... [et al.]6-MeV Electron Exposure Effects on OFDR-Based Distributed Fiber-Based Sensors. (2018) IEEE Transactions on Nuclear Science, 65 (8). 1598-1603. ISSN 0018-9499

Any correspondence concerning this service should be sent to the repository administrator:

[tech-oatao@listes-diff.inp-toulouse.fr](mailto:tech-oatao@listes-diff.inp-toulouse.fr)

# 6-MeV Electron Exposure Effects on OFDR-Based Distributed Fiber-Based Sensors

Camille Sabatier<sup>1b</sup>, *Student Member, IEEE*, Serena Rizzolo<sup>2b</sup>, *Member, IEEE*,  
Adriana Morana<sup>3b</sup>, *Member, IEEE*, Timoth e Allanche<sup>1b</sup>, *Student Member, IEEE*, Thierry Robin,  
Benoit Cadier, Philippe Paillet, *Fellow, IEEE*, Marc Gaillardin<sup>1b</sup>, *Member, IEEE*, Olivier Duhamel,  
Claude Marcandella, Damien Aubert, Gilles Assaillit, G erard Auriel, Aziz Boukenter,  
Youcef Ouerdane, Luciano Mescia, Emmanuel Marin, and Sylvain Girard<sup>1b</sup>, *Senior Member, IEEE*

**Abstract**—The impact of exposing an optical fiber to 6-MeV electrons on the performances of optical frequency domain reflectometry (OFDR) distributed sensors is investigated. Six different types of optical fibers with different core compositions and coatings have been tested: four fibers are metal coated (copper, gold, or aluminum) for high-temperature (>300 °C) operations while the two others have telecom-grade acrylate coatings for operation below 80 °C. The fiber Rayleigh signature used to perform the OFDR sensing remains almost unaffected after an electron exposure. Indeed, the measured radiation-induced temperature errors are lower than about 3 °C, close to the setup uncertainties, when the OFDR operates as a temperature sensor.

**Index Terms**—Dose, dose rate temperature, electrons, fiber sensor, optical frequency domain reflectometry (OFDR), optical fiber, radiation, Rayleigh scattering.

## I. INTRODUCTION

OPTICAL fiber sensors (OFSs) have attracted much attention, thanks to their many advantages compared with conventional electrical sensors. The optical fibers are lightweight, the dielectric nature of silica renders them immune to most of the electromagnetic perturbations and they offer distributed sensing capabilities when combined with reflectometry techniques [1]. Different classes of optical fiber sensors, mainly for temperature or strain monitoring, have been developed: punctual ones such as fiber Bragg gratings [2], [3], or distributed ones such as those exploiting the Brillouin [4], Raman [5], and Rayleigh [6], [7] scattering

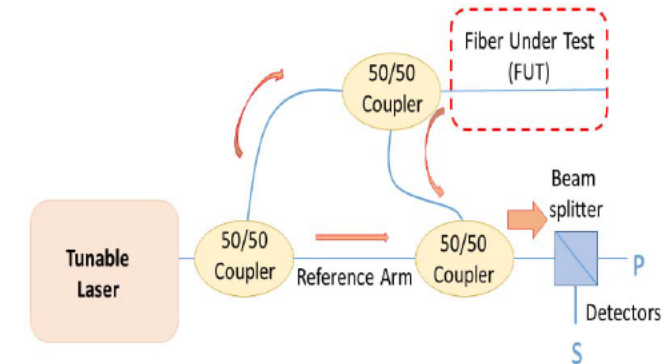


Fig. 1. Schematic of the OFDR network.

signatures of the silica-based fibers. Since for most of those technologies, the radiation influences the OFS response when the fiber is submitted to this constraint (while the interrogator can be placed in a radiation-free zone), several recent studies have been performed to enhance their radiation resistance by improving the fibers themselves or acting at the interrogation system architecture levels to reduce the radiation impact on the measure [8]–[10].

If most of studies focused on radiation-hardened optical fibers, it must be noticed that some radiation-sensitive fibers have been identified as promising candidates for dosimetry cartographies [11]–[14]. Among all the various distributed OFS technologies, we recently demonstrated, in [9] and [10], that the Rayleigh scattering signature exploited by the optical frequency domain reflectometry (OFDR) sensors appear as mostly radiation insensitive at least up to 10 MGy (SiO<sub>2</sub>) total ionizing doses (TID) of X-rays or  $\gamma$ -rays. Fig. 1 illustrates the operation principle of the OFDR technique. The OFDR technique is an evolution of the optical time domain reflectometry (OTDR) technique that was investigated in the past for operation in radiation environments [14] and today for radiation dosimetry at CERN [13]. The light issued from a tunable laser is split between a reference arm and another arm comprising the fiber under test (FUT). When the backscattered lights from the FUT and the reference arm are mixed together, they generate an interference pattern which is detected through two detectors (labeled P and S in Fig. 1) in two orthogonal

C. Sabatier is with the Laboratory Hubert Curien, CNRS UMR 5516, Universit e de Lyon, 42000 Saint- tienne, France, also with ixBlue Photonics, 22300 Lannion, France, and also with the Politecnico di Bari, 70126 Bari, Italy (e-mail: camille.sabatier@univ-st-etienne.fr).

S. Rizzolo is with ISAE-SUPAERO, 31055 Toulouse, France.

A. Morana, T. Allanche, A. Boukenter, Y. Ouerdane, E. Marin, and S. Girard are with the Laboratoire Hubert Curien, CNRS UMR 5516, Universit e de Lyon, 42000 Saint- tienne, France (e-mail: sylvain.girard@univ-st-etienne.fr).

T. Robin and B. Cadier are with ixBlue Photonics, 22300 Lannion, France. P. Paillet, M. Gaillardin, O. Duhamel, and C. Marcandella are with CEA/DAM/DIF, 91680 Arpajon, France.

D. Aubert, G. Assaillit, and G. Auriel are with the CEA DAM/centre de Gramat, 46500 Gramat, France.

L. Mescia is with Politecnico di Bari, 70126 Bari, Italy.

Color versions of one or more of the figures in this paper are available online at <http://ieeexplore.ieee.org>.

Digital Object Identifier 10.1109/TNS.2018.2804663

polarization states [16]. Doing a Fourier transform renders the possibility to obtain the fiber scattering signature (that is unique for each fiber sample) with a spatial resolution better than 1 mm along the whole length (up to 70 m) of the FUT while the spatial resolution of OTDR sensors is typically of 1 m [17]. The external constraints (temperature, radiation, or strain changes) stimulate the fiber material changing locally its refractive index distribution along the FUT length. The local perturbation modifies then the backscattered signal too.

OFDRs are able to monitor these changes by performing a cross correlation between the perturbed state and a well-defined state for which all the environmental parameters are known (called reference state). The result of this cross correlation gives information about the spectral shift caused by the applied perturbation with respect to the initial conditions from the reference state. The spectral shift monitoring as a function of the fiber length allows calculating the stimuli amplitude through [17]

$$\frac{\Delta\lambda}{\lambda_c} = -\frac{\Delta\nu}{\nu_c} = C_T \cdot \Delta T + C_\varepsilon \cdot \varepsilon \quad (1)$$

where  $\lambda_c$  and  $\nu_c$  are the central wavelength and frequency,  $C_T$  and  $C_\varepsilon$  are the temperature and strain coefficients of the sensing fiber, which have to be obtained by calibrating the sensor before its integration, and  $\Delta T$  and  $\varepsilon$  are the temperature variation and the fiber applied strain between the reference and perturbed states. We studied in this paper, the OFDR-based sensor response when its sensing fiber is exposed to 6-MeV electrons. In particular, six fibers, having different compositions (germanium or fluorine doping in core) and different coatings (acrylate or metal coatings), are investigated up to an equivalent TID of  $\sim 1.6$  MGy(SiO<sub>2</sub>). The objective of this paper is to evaluate whether the Rayleigh signature of the various fibers is affected by the 6-MeV electrons. If, as for the X-rays and  $\gamma$ -rays [9], [10], the Rayleigh signature remains unaffected by radiations, it will open the way to the design of OFDR sensors to operate either as temperature sensors in electron-rich, high-temperature environments (*high-energy physics facilities or space environments*) or as highly spatially resolved beam profilers when using radiation sensitive optical fibers for cartographies of electron beams through measurements of the radiation-induced attenuation, as discussed in [12] and [18] for  $\gamma$ -rays.

## II. MATERIALS AND METHODS

An optical backscatter reflectometer (OBR) (OBR4600 from Luna Technologies) was used for these tests. It operates with a central wavelength ( $\lambda_c$ ) of 1550 nm and a spectral width of 43 nm, allowing to achieve a spatial resolution up to 20  $\mu$ m. Six different samples have been tested.

### A. Impact of Prethermal Treatment on Rayleigh Response

Four fibers have a germanium-doped core, a pure silica cladding, and different coatings: acrylate (SMFGe\_ac), aluminum (SMFGe\_Al), copper (SMFGe\_Cu), and gold (SMFGe\_Au), which are able to operate up to 80  $^\circ$ C, 400  $^\circ$ C, 450  $^\circ$ C, and 700  $^\circ$ C, respectively. The other two fibers have been doped with fluorine in both core and cladding,

TABLE I  
MAIN CHARACTERISTICS OF THE SAMPLES

Core dopant	Sample name	Coating	$C_T$ ( $10^{-6}C^{-1}$ ) treated	$C_T$ ( $10^{-6}C^{-1}$ ) untreated
Germanium	SMFGe_Ac	Acrylate	6.70 $\pm$ 0.03	6.64 $\pm$ 0.03
	SMFGe_Cu	Copper	10.16 $\pm$ 0.12	9.49 $\pm$ 0.11
	SMFGe_Au	Gold	9.67 $\pm$ 0.07	8.81 $\pm$ 0.07
	SMFGe_Al	Aluminum	12.6 $\pm$ 0.4	8.6 $\pm$ 0.4
Fluorine	SMFF_Ac	Acrylate	6.71 $\pm$ 0.05	6.48 $\pm$ 0.06
	SMFF_Al	Aluminum	11.9 $\pm$ 0.8	8.4 $\pm$ 0.6

one is coated with acrylate (SMFF\_ac) and the other with aluminum (SMFF\_Al). For each fiber type, two samples were irradiated: one untreated and the other that underwent to a cycle of four thermal treatments. Indeed, it has been shown in [19] that these thermal treatments stabilize the temperature coefficients of optical fibers with polymer-based coatings, and then ameliorates the sensor performances in terms of temperature measurements. Consequently, before the irradiation we performed on samples of all fibers, in a stress-free configuration, four thermal treatments from 30  $^\circ$ C to 80  $^\circ$ C (with a step of 10  $^\circ$ C). Each step lasted 30 min to reach a stabilization of the oven temperature within 1  $^\circ$ C. Between two consecutive runs, the temperature went down to 30  $^\circ$ C naturally. The spectral shift was recorded during the thermal treatments, in order to calculate the sample temperature coefficient. This coefficient corresponds to an average value of the results obtained for ten different points located along each fiber length. Table I reports the main characteristics of the samples untreated and treated. The temperature coefficients  $C_T$ , here reported, are obtained as the mean of the  $C_T$  values in the 10 points, whereas the associated error corresponds to the standard deviation. The  $C_T$  of the untreated and treated samples are obtained during the first treatment and the fourth treatment, respectively.

We can observe that the error bars associated with the  $C_T$  of the aluminum-coated fibers are larger than those of other samples. This can be explained by a larger dispersion in the responses of the 10 points for such fibers, an effect that is assumed to be related to a longitudinal inhomogeneity of the coating-fiber interface [20].

Fig. 2 shows the evolution of thermal coefficients as a function of the number of performed thermal treatments. We can observe larger variations of  $C_T$  for SMFGe\_Al (47%) and SMFF\_Al (42%) between the first and the last thermal treatment. The  $C_T$  variations for the SMFGe\_ac (0.9%) SMFGe\_Cu (7%), SMFGe\_Au (10%), and SMFF\_ac (4%) are less important. After four thermal treatments, the coefficients are stable for all tested fibers.

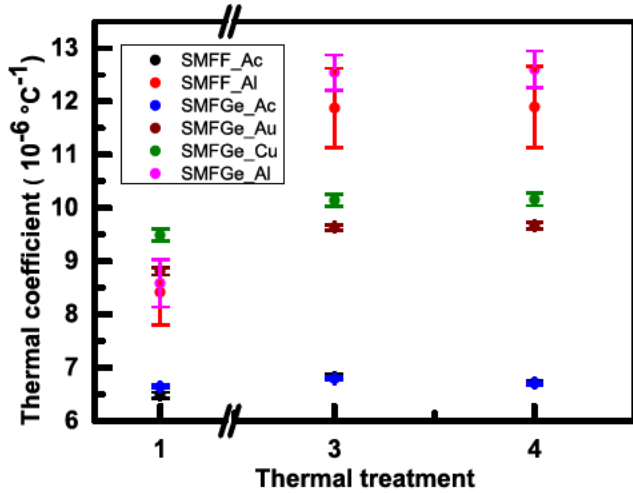


Fig. 2. Impact of thermal treatments on the temperature sensitivity coefficients of all tested fibers. Because of a problem with the acquisition system, the data of the second thermal treatment are missing, but they are not crucial to highlight the  $C_T$  stabilization process.

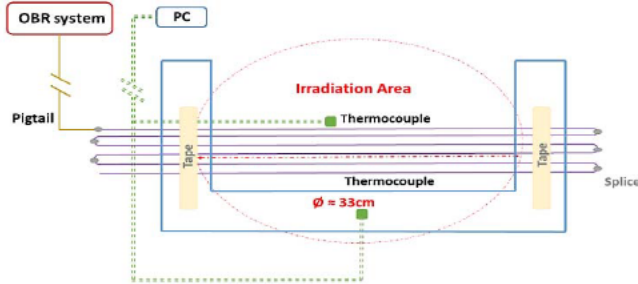


Fig. 3. Experimental setup. The fibers were fixed in series on a plexiglas plate without the applied strain. The temperature of the fibers was monitored with two thermocouples. The electron beam was perpendicular to the fibers. These fibers were interrogated by the OBR4600.

### B. Irradiation Session

The irradiation facility used for this paper is the ORIATRON machine from CEA DAM, Gramat, France. This facility delivers electrons with an average energy of 6 MeV, in a quasi-CW mode: the electron beam is a train of 4.5- $\mu$ s pulses at a frequency of 250 Hz [21].

During the irradiation, as shown in Fig. 3, each type of optical fiber thermally treated and untreated were spliced with each other in series and to a pigtail, to be connected to the OBR. The irradiated part of the optical fiber part was maintained as stress-free as possible, in order to reduce the dilatation effects occurring during the irradiation because of the temperature increase. The fibers were maintained in the same position, thanks to Kapton adhesive tape positioned outside the irradiation area on a Plexiglas plate with the shape shown in Fig. 3. To study the radiation-induced effect on the Rayleigh response, only the stress-free fiber part was considered for analysis.

The samples were placed at 1.6-m distance from the radiation source; at this distance, the dose rate was of about 120 Gy/s, whereas electron beam has a diameter of about 33 cm (area between the two tape bands). The spectral shift was recorded before (used as the reference) and after the

irradiation, with a selected spatial resolution of 5 mm. Due to the excess of ozone in the irradiation chamber during the electron irradiation, the experiment was divided in consecutive runs over two days. The dose accumulated in each run lasting approximately 15 min was about 108 kGy, whereas the TID was 1.6 MGy.

To study the permanent radiation effects, for each sample, the spectral shift of a zone of about 4-cm length, placed in correspondence with the electron beam maximum, was acquired with a spatial resolution of 5 mm. The mean and the standard deviation of the spectral shift for the whole fiber length are calculated as a function of the accumulated dose.

Since the temperature variation in the irradiation room will cause a spectral shift, as reported in (1), two type-K thermocouples (TCs) were placed as close as possible to the samples to monitor the room temperature evolution during the experiments. Since it has been demonstrated that the temperature coefficient is not influenced by  $\gamma$ -rays up to 10 MGy [19], the temperature-induced contribution, calculated with the values of  $C_T$  measured before irradiation, was subtracted from the recorded spectral shift in order to highlight the sole radiation-induced effects.

## III. EXPERIMENTAL RESULTS

### A. Impact of Prethermal Treatment on Rayleigh Response Under Irradiation

The next figures report the permanent spectral shift recorded after each run as a function of the accumulated dose. Despite the fact that our setup should allow the monitoring of the transient (or *in situ*) spectral shifts, our results pointed out that the electrons affected the TCs by degrading strongly their signal-to-noise levels. As a consequence, during the run, the quite large observed fluctuations of temperature (more than 10 °C) cannot be efficiently subtracted to highlight the sole radiation effects. Even after irradiation, it was necessary to wait about 10 min that the stabilization of the TC temperature is achieved before acquiring the OFDR traces. With these conditions, only small temperature variations, of less than 1 °C, exist between the references and new states. Such small changes can be corrected, thanks to (1) and the  $C_T$  values of Table I.

Fig. 4 compares the dose dependence of the spectral shifts of two fiber samples, one untreated and another pretreated. The results for the F-doped fiber with acrylate coating are given in Fig. 4(a) while those of Ge-doped one with copper coating are given in Fig. 4(b).

Concerning the copper fiber [Fig. 4(b)], the OFDR response is quite similar for both samples. The average spectral shift recorded after the irradiation runs is  $0.7 \times 10^{-5}$  (which corresponds to an error in the temperature measurements of about 0.7 °C) for the untreated fiber and  $0.6 \times 10^{-5}$  (0.6 °C) for the treated one. The maximum spectral shift difference between treated and untreated fibers during the entire experiment is only  $0.6 \times 10^{-5}$ , which is less than 0.6 °C. For the SMFF\_ac [Fig. 4(a)], the average spectral shift is lower for the treated sample ( $-0.16 \times 10^{-5}$ ) than for the untreated one ( $-0.4 \times 10^{-5}$ ), corresponding to a temperature

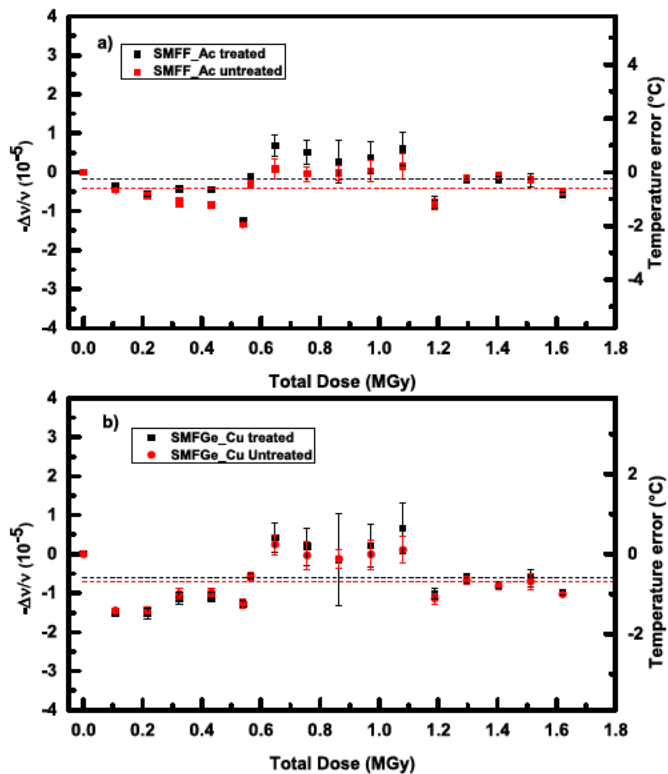


Fig. 4. Dose dependence of the permanent radiation-induced spectral shift (a) SMFF\_ac and (b) SMFGe\_Cu, treated (black squares) and untreated (red circles). Dashed dotted line: mean spectral shift.

error of 0.2 °C and 0.6 °C, respectively. The maximum spectral shift difference between treated and untreated fibers is of about  $0.7 \times 10^{-5}$  (less than 1 °C). Table II reports the Rayleigh response for the other treated and untreated optical fibers. For SMFGe\_Al and SMFF\_Al the thermal treatment slightly impacts their radiation responses, the maximum spectral shift difference between treated and untreated is  $1.5 \times 10^{-5}$  (1.2 °C) for SMFGe\_Al and  $2.6 \times 10^{-5}$  (2.2 °C) for SMFF\_Al. This difference with other samples can be explained by the quality of coating. We have shown in the precedent part that the coating–fiber interface could be inhomogeneous. Concerning the sample with other coatings than Al, the maximum spectral shift between treated and untreated remains lower than  $10^{-5}$  (approximately 1 °C). According to these results, it appears that pretreating the optical fibers may not mandatory to guarantee good performances (temperature error below 1 °C) of this OFS under electron irradiation for temperatures between 20 °C and 40 °C. In Sections III-B and III-C, we then focus on pretreated fibers.

### B. Impact of Radiation on Fibers With Different Coatings and Dopants

In order to evaluate the electron-induced effects, Fig. 5 reports the evolution of the radiation-induced spectral shift, corrected for the temperature fluctuations, for each fiber as a function of TID. The responses of the F-doped and Ge-doped optical fibers are given in Fig. 5(a) and (b), respectively. Table III shows the average spectral shift, the maximum recorded values, and the amplitude of the variations.

TABLE II  
DIFFERENT RAYLEIGH RESPONSES BETWEEN TREATED AND UNTREATED OPTICAL FIBERS

Sample	Mean spectral shift ( $10^{-5}$ )	Related Temperature error (°C)	Maximum spectral shift difference between treated & untreated ( $10^{-5}$ )
SMFGe_Ac treated	0.3	0.4	Not available
SMFGe_Ac Untreated	not available	Not available	
SMFGe_Cu treated	0.6	0.6	0.6 (0.6°C)
SMFGe_Cu Untreated	0.7	0.7	
SMFGe_Au treated	-0.9	-0.9	0.8 (0.8°C)
SMFGe_Au Untreated	-1.2	1.4	
SMFGe_Al treated	-1.2	1	1.5 (1.2°C)
SMFGe_Al Untreated	-1.6	1.9	
SMFF_Ac treated	-0.16	-0.2	0.6 (0.9°C)
SMFF_Ac Untreated	-0.4	-0.6	
SMFF_Al treated	0.7	0.6	2.6 (2.2°C)
SMFF_Al Untreated	-0.3	-0.4	

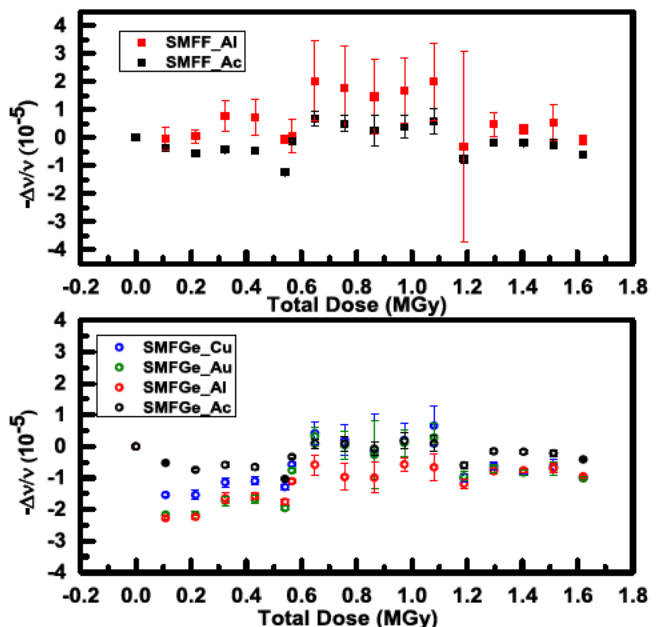


Fig. 5. Dose dependence of the permanent radiation-induced spectral shift. (a) F-doped and (b) Ge-doped optical fibers with different types of coatings.

The SMFGe\_ac fiber with an acrylate coating presents the lower average spectral shift compared with the other germanosilicate fibers. Indeed, all the metal-coated fibers are characterized by an average spectral shift, which is at least

TABLE III  
MAXIMUM SPECTRAL SHIFT INDUCED DURING THE IRRADIATION  
AFTER CORRECTION OF THE TEMPERATURE FLUCTUATIONS

Fiber name	Type of coating	Mean ( $-\Delta\nu/\nu$ ) ( $10^{-5}$ )	Range of min / max values ( $10^{-5}$ )	Amplitude Range ( $10^{-5}$ )
SMFGe_Ac	Acrylate	-0.3	-1/0.2	1.2
SMFGe_Cu	Copper	-0.6	-1.5/0.6	2.1
SMFGe_Au	Gold	-0.8	-2.2/0.3	2.5
SMFGe_Al	Aluminum	-1.1	-2.3/-0.6	1.7
SMFF_Ac	Acrylate	-0.2	-1/0.6	1.6
SMFF_Al	Aluminum	-0.7	-0.3/2	2.3

twice the value of SMFGe\_ac. Moreover, the Ge-doped fiber with acrylate has the smallest range of amplitude. Concerning the F-doped fibers, the average spectral shift and the amplitude range associated with the acrylate-coated sample (SMFF\_ac) are smaller than those of the aluminum-coated one (SMFF\_Al). From our tests, the metal coatings seem associated with higher permanent radiation-induced spectral shifts than acrylate ones. For operation in electron-rich environments, SMFGe\_ac and SMFF\_ac fibers appear as the most promising candidates for temperature measurements with the limitation that the irradiation temperature has to remain below 80 °C; otherwise, the use of metal-coated fibers is mandatory.

The radiation-induced spectral shift measured for the metal-coated samples could be at least partially explained by its visible electron-induced oxidation. Such effect was clearly observed for the copper- and gold-coated samples.

To highlight the effects of the core dopants, we can compare the spectral shifts of the two samples with acrylate coatings (SMFGe\_ac and SMFF\_ac) and the two samples with aluminum coatings (SMFGe\_Al and SMFF\_Al). Independent of the coating nature, the F-doped fibers show lower average spectral shift (of about 30%) but a larger amplitude range (of about 25%), compared with the Ge-doped samples. Then, the dopant choice does not influence clearly the Rayleigh response under electron irradiation.

### C. Error in Temperature Measurements

In order to evaluate the OFDR sensor performances when using these fibers as temperature sensors, Fig. 6 and Table IV report the temperature error due to the radiation effects on spectral shift: this error is calculated, thanks to (1) by using the  $C_T$  value of the treated samples in Table I.

As expected, the metal-coated fibers are associated with the larger errors caused by the larger radiation-induced Rayleigh spectral shift. For both fiber compositions, the acrylate-coated fibers are associated with the lower temperature error ( $-0.45$  °C for SMFGe\_ac and  $-0.3$  °C for SMFF\_ac) than the metal-coated ones. Concerning the range of amplitude, the aluminum-coated Ge-doped fiber, SMFGe\_Al, presents the lowest value, only 1.3 °C.

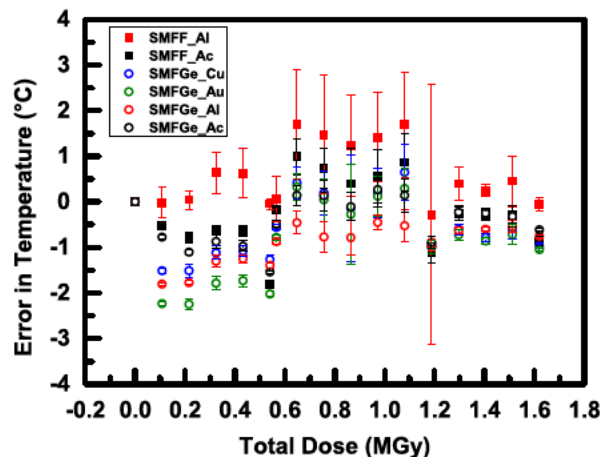


Fig. 6. Equivalent temperature errors due to the radiation-induced spectral shift as a function of the TID for fibers with different core compositions and different types of coatings.

TABLE IV  
TEMPERATURE ERROR DUE TO THE ELECTRON IRRADIATION EXPOSURE

Fiber name	Type of coating	Mean (°C)	Range of Min/max values (°C)	Amplitude Range (°C)
SMFGe_Ac	Acrylate	-0.45	-1.5/0.3	1.8
SMFGe_Cu	Copper	-0.6	-1.5/0.6	2.1
SMFGe_Au	Gold	-0.8	-2.3/0.3	2.6
SMFGe_Al	Aluminum	-0.9	-1.8/-0.5	1.3
SMFF_Ac	Acrylate	-0.3	-1.5/0.9	2.4
SMFF_Al	Aluminum	0.6	-0.3/1.7	2.0

As shown in Section III-B, the acrylate-coated F-doped fiber gives lower mean temperature error but larger dispersion than the Ge-doped fiber. Same conclusions can be stated for the aluminum-coated samples, SMFF\_Al and SMFGe\_Al. In conclusion, the acrylate appears as a more adapted coating than the metal-based ones for operation below 80 °C. Metal-coated fibers can probably be used efficiently at higher temperature. An important result is that the fiber composition does not influence significantly the OFDR performances, at least for F- and Ge-doped fibers. It is then possible to select the fiber composition in order to minimize the issues related to radiation-induced attenuation [22] if the measurements have to be done on long distances of fibers at high-dose rate/dose or to maximize it for dosimetry purposes.

## IV. CONCLUSION

We studied the impact of irradiating an optical fiber with 6-MeV electrons on the OFDR sensor performances. Six different fibers were tested as the sensor sensitive element: four have a Ge-doped core and two have an F-doped core. Some F-doped and Ge-doped samples have an acrylate coating while

others have aluminum coatings. Two additional Ge-doped samples, one coated with copper and the other with gold, were also tested under the same conditions. It was observed that the OFDR sensing properties remain stable after the electron irradiation for all the different fibers, with a maximum variation of their spectral shift due to the radiations measured of about  $2.2 \times 10^{-5}$  for the gold-coated Ge-doped fiber. For this fiber, this corresponds to a temperature error of  $-2.3$  °C if the sensor is used for temperature monitoring.

The fiber composition does not influence the OFDR sensor performances. The metal-based coatings, instead, seem to slightly increase the radiation-induced spectral shift and then the associated temperature error. This may be at least partially explained by the oxidation, clearly visible after the electron beam exposure, of the copper- and gold-coated samples.

The *ex situ* performances of OFDR sensors are almost unaffected by electron irradiation; indeed, the estimated radiation-induced temperature errors are lower than about 3 °C, between 1.7 °C (SMFF\_Al) and  $-2.3$  °C (SMFGe\_Au) at MGy dose levels. Future experiments will have to be performed to ensure that the reported results and discussion remain valid during the electron irradiation, even if this assumption seems reasonable as potential structural changes induced by electrons should be stable at room temperature. As the electron irradiation is accompanied by a temperature increase of the sample and radiation-induced attenuation, the potential of the OFDR sensing technique to monitor the electron beam profile with a spatial resolution down to a few millimeters will be investigated.

## REFERENCES

- [1] X. Bao and L. Chen, "Recent progress in distributed fiber optic sensors," *Sensors*, vol. 12, no. 7, pp. 8601–8639, Jun. 2012.
- [2] A. Morana *et al.*, "Radiation tolerant fiber Bragg gratings for high temperature monitoring at MGy dose levels," *Opt. Lett.*, vol. 39, no. 18, pp. 5313–5316, Sep. 2014.
- [3] A. Faustov, "Advanced fibre optics temperature and radiation sensing in harsh environments," Ph.D. dissertation, Univ. Mons, Mons, Belgium, 2014.
- [4] X. Phéron *et al.*, "High  $\gamma$ -ray dose radiation effects on the performances of Brillouin scattering based optical fiber sensors," *Opt. Exp.*, vol. 20, no. 24, pp. 26978–26985, 2012.
- [5] C. Cangialosi *et al.*, "Development of a temperature distributed monitoring system based on Raman scattering in harsh environment," *IEEE Trans. Nucl. Sci.*, vol. 61, no. 6, pp. 3315–3322, Dec. 2014.
- [6] A. V. Faustov, A. Gusarov, L. B. Liokumovich, A. A. Fotiadi, M. Wuilpart, and P. Mégret, "Comparison of simulated and experimental results for distributed radiation-induced absorption measurement using OFDR reflectometry," *Proc. SPIE*, vol. 8794, p. 879430, May 2013.
- [7] S. T. Kreger *et al.*, "High-resolution extended distance distributed fiber-optic sensing using Rayleigh backscatter," *Proc. SPIE*, vol. 6530, p. 65301R, Apr. 2007.
- [8] S. Rizzolo, "Advantages and limitation of distributed OFDR optical fiber-based sensors in harsh environments," Ph.D. dissertation, Jean Monnet Univ., Saint-Étienne, France, 2016.
- [9] S. Rizzolo *et al.*, "Vulnerability of OFDR-based distributed sensors to high  $\gamma$ -ray doses," *Opt. Exp.*, vol. 23, no. 15, pp. 18997–19009, Jul. 2015.
- [10] S. Rizzolo *et al.*, "Radiation effects on optical frequency domain reflectometry fiber-based sensor," *Opt. Lett.*, vol. 40, no. 20, pp. 4571–4574, 2015.
- [11] S. Girard, Y. Ouerdane, C. Marcandella, A. Boukenter, S. Quenard, and N. Authier, "Feasibility of radiation dosimetry with phosphorus-doped optical fibers in the ultraviolet and visible domain," *J. Non-Cryst. Solids*, vol. 357, nos. 8–9, pp. 1871–1874, Apr. 2011.
- [12] A. V. Faustov *et al.*, "Application of phosphate doped fibers for OFDR dosimetry," *Results Phys.*, vol. 6, pp. 86–87, Jan. 2016.
- [13] I. Toccacafondo *et al.*, "Distributed optical fiber radiation sensing in a mixed-field radiation environment at CERN," *J. Lightw. Technol.*, vol. 37, pp. 3303–3310, Aug. 15, 2017.
- [14] D. Di Francesca *et al.*, "Distributed optical fiber radiation sensing in the proton synchrotron booster at CERN," *Trans. Nucl. Sci.*, no. 99, Mar. 2018, doi: [10.1109/TNS.2018.2818760](https://doi.org/10.1109/TNS.2018.2818760).
- [15] H. Henschel, O. Kohn, and H. U. Schmidt, "Radiation induced loss measurements of optical fibres with optical time domain reflectometers (OTDR) at high and low dose rates," in *Proc. 1st Eur. Conf. Radiat. Effects Devices Syst. (RADECS)*, Sep. 1991, pp. 380–382.
- [16] S. T. Kreger, D. K. Gifford, M. E. Froggatt, B. J. Soller, and M. S. Wolfe, "High resolution distributed strain or temperature measurements in single- and multi-mode fiber using swept-wavelength interferometry," in *Proc. Opt. Fiber Sensors*, 2006, paper ThE42, doi: [10.1364/OFS.2006.ThE42](https://doi.org/10.1364/OFS.2006.ThE42).
- [17] M. E. Froggatt and J. Moore, "High-spatial-resolution distributed strain measurement in optical fiber with Rayleigh scatter," *Appl. Opt.*, vol. 37, no. 10, pp. 1735–1740, 1998.
- [18] A. V. Faustov *et al.*, "The use of optical frequency-domain reflectometry in remote distributed measurements of the  $\gamma$ -radiation dose," *Tech. Phys. Lett.*, vol. 41, no. 5, pp. 414–417, May 2015.
- [19] S. Rizzolo *et al.*, "Radiation characterization of optical frequency domain reflectometry fiber-based distributed sensors," *IEEE Trans. Nucl. Sci.*, vol. 63, no. 3, pp. 1688–1693, Jun. 2016.
- [20] Y.-S. Shiue, M. J. Matthewson, C. R. Kurkjian, and D. R. Biswas, "Strength and surface characterization of aluminum-coated fused silica fibers," *Proc. SPIE*, vol. 2611, pp. 117–121, Jan. 1996.
- [21] D. Aubert *et al.*, "A 6 MeV electron linac facility for multipurpose radiation testing," in *Proc. Eur. Conf. Radiat. Effects Devices Syst. (RADECS)*, Bremen, Germany, Sep. 2016, pp. 1–3, doi: [10.1109/RADECS.2016.8093158](https://doi.org/10.1109/RADECS.2016.8093158).
- [22] S. Girard *et al.*, "Radiation effects on silica-based optical fibers: Recent advances and future challenges," *IEEE Trans. Nucl. Sci.*, vol. 60, no. 3, pp. 2015–2036, Jun. 2013.